Development/Plasticity/Repair

Mice Deficient in Collapsin Response Mediator Protein-1 Exhibit Impaired Long-Term Potentiation and Impaired Spatial Learning and Memory

Kang-Yi Su,[1,2] Wei-Lin Chien,[3]* Wen-Mei Fu,[3] I-Shing Yu,[2]* Hsiang-Po Huang,[4] Pei-Hsing Huang,[5] Shu-Rung Lin,[8] Jin-Yuan Shih,[6] Yi-Ling Lin,[9] Yi-Ping Hsueh,[9] Pan-Chyr Yang,[6] and Shu-Wha Lin[2,7]

[1]Institute of Molecular Medicine, and Departments of [2]Clinical Laboratory Sciences and Medical Biotechnology, [3]Pharmacology, [4]Medical Research, [5]Pathology, [6]Internal Medicine, and [7]Laboratory Medicine, National Taiwan University Hospital, College of Medicine, National Taiwan University, Taipei 100, Taiwan, [8]Department of Bioscience Technology, College of Science, Chung-Yuan Christian University, Taoyuan 320, Taiwan, and [9]Institute of Molecular Biology, Academia Sinica, Taipei 115, Taiwan

Collapsing response mediator protein-1 (CRMP-1) was initially identified in brain and has been implicated in plexin-dependent neuronal function. The high amino acid sequence identity among the five CRMPs has hindered determination of the functions of each individual CRMP. We generated viable and fertile *CRMP-1* knock-out (*CRMP-1*$^{-/-}$) mice with no evidence of gross abnormality in the major organs. *CRMP-1*$^{-/-}$ mice exhibited intense microtubule-associated protein 2 (MAP2) staining in the proximal portion of the dendrites, but reduced and disorganized MAP2 staining in the distal dendrites of hippocampal CA1 pyramidal cells. Immunoreactivity to GAP-43 (growth-associated protein-43) and PSD95 (postsynaptic density-95) (a postsynaptic membrane adherent cytoskeletal protein) was also decreased in the CA1 region of the knock-out mice. These changes were consistent with the mutant mice showing a reduction in long-term potentiation (LTP) in the CA1 region and impaired performance in hippocampal-dependent spatial learning and memory tests. *CRMP-1*$^{-/-}$ mice showed a normal synapsin I labeling pattern in CA1 and normal paired-pulse facilitation. These findings provide the first evidence suggesting that CRMP-1 may be involved in proper neurite outgrowth in the adult hippocampus and that loss of CRMP-1 may affect LTP maintenance and spatial learning and memory.

Key words: **CRMP-1; knock-out mice; Cre recombinase; loxP; Morris water maze; long-term potentiation**

Introduction

The collapsin response mediator protein (CRMP) family consists of five gene products (CRMP-1∼CRMP-5) of similar molecular size (60–66 kDa), with a high (50–70%) amino acid sequence identity (Goshima et al., 1995; Byk et al., 1996; Wang and Strittmatter, 1996; Gaetano et al., 1997; Quinn et al., 1999; Fukada et al., 2000). CRMPs are intracellular phosphoproteins predominantly expressed in the nervous system during development (Goshima et al., 1995; Gaetano et al., 1997; Byk et al., 1998; Quach et al., 2004). They play a role in repulsive guidance of growth cones (Quinn et al., 1999), a function that is critical for normal growth and development of neurons and thus ultimately required for proper formation of neuroanatomy and synaptic connections (Liu and Strittmatter, 2001). Although the molecular mechanisms mediating this function have not yet been fully characterized (Quinn et al., 1999), evidence suggests that CRMP-1, CRMP-2, and CRMP-5 may regulate axon outgrowth via interactions with semaphorin signaling pathways to affect the dynamics of microtubules and induce collapse of neuronal growth cones (Gu and Ihara, 2000). CRMP-1 and CRMP-2 interact with tubulin dimers (Shih et al., 2001; Fukata et al., 2002), and CRMP-2 interaction with tubulin dimers has been shown to promote microtubule assembly for neurite elongation (Fukata et al., 2002). Moreover, CRMP-2 links tubulin dimers with Sra-1 and kinesin-1 as a cargo adaptor to regulate their transport in neurites

Received May 19, 2006; revised Jan. 23, 2007; accepted Jan. 23, 2007.

This work was supported by National Science Council Grants NSC93-3112-B002-039, NSC94-2320-B002-092, NSC94-3112-B002-014, NSC95-2752-B002-011-PAE, and NSC95-2752-B006-003-PAE; National Health Research Institute Grants NHRI-EX90-9142SI, NHRI-EX91-9142SI, and NHRI-EX92-9192SI; and National Taiwan University Hospital Grants 90A01, 91A06, and 92A10-7. We thank Ying-Hui Su and Hui-Yu Tseng for their excellent technical assistance, and Chiu-Wen Yeh, Ying-Chien Wang, and Ching-Wen Yang for animal care. We also thank Prof. Alice Chien Chang (Institute of Neuroscience, National Yang-Ming University, Taipei, Taiwan) and Dr. Chih-Cheng Chen (Institute of BioMedical Sciences, Academia Sinica, Taipei, Taiwan) for their helpful discussions. We thank Dr. Chin-Chin Huang (Chia-Yi University, Chia-Yi City, Taiwan) for her contribution, as well as Prof. Jau-Tsuen Kao [Department of Clinical Laboratory Science and Medical Biotechnology, National Taiwan University Medical Center (NTUMC), Taipei, Taiwan] and Dr. Shyh-Chyi Lo [Department of Laboratory Medicine, National Taiwan University Hospital (NTUH), Taipei, Taiwan] for their support with the Clinical Chemistry and Blood Bank facilities. We appreciate the generosity of Prof. Keng-Chen Liang (Department of Psychology, National Taiwan University, Taipei, Taiwan) for providing the facility for behavioral testing, the knock-out Mouse Core Facility at the Center for Genomic Medicine (NTUMC) and the Transgenic Mouse Model Core Facility of the National Research Program for Genomic Medicine for the generation of CRMP-1 null mice, and Shu-Chen Shen (Department of Medical Research, NTUH) for availability and assistance with the confocal microscope facility.

*W.-L.C. and I.-S.Y. contributed equally to this work.

Correspondence should be addressed to either of the following: Dr. Shu-Wha Lin, Department of Clinical Laboratory Sciences and Medical Biotechnology, College of Medicine, National Taiwan University, Number 7, Chung-San South Road, Taipei 100, Taiwan. E-mail: mtshuwha@ccms.ntu.edu.tw; or Dr. Pang-Chyr Yang, Department of Internal Medicine, College of Medicine, National Taiwan University, Number 7, Chung-San South Road, Taipei 100, Taiwan. E-mail: pcyang@ha.mc.ntu.edu.tw.

DOI:10.1523/JNEUROSCI.4497-06.2007

 0270-6474/07/272513-12$15.00/0

(Arimura and Kaibuchi, 2005). Thus, disruption of CRMP function and semaphorin signaling pathways may disrupt neural growth and development (Chen et al., 2000; Cheng et al., 2001).

The role of CRMP-1 in neural development and growth cone collapse has not been well characterized. Expression of CRMP-1, like the other CRMPs, peaks from the late embryonic stage to postnatal day 15 (P15), with the highest levels being observed in the forebrain and lesser levels in the cerebellum (Wang and Strittmatter, 1996). After this peak in developmental expression, CRMP-1 is constitutively expressed at lower levels throughout adulthood (Wang and Strittmatter, 1996). The persistent expression of CRMP-1 and several other CRMPs in the hippocampus and the cerebellum throughout adulthood implies that they may play a role in adults. For example, CRMP-2 was found to be associated with neurofibrillary tangles in patients with Alzheimer's disease (Good et al., 2004; Uchida et al., 2005). CRMP-3 and CRMP-5 are recognized by autoantibodies from patients with small-cell lung carcinoma with paraneoplastic neurological syndrome (Honnorat et al., 1999; Yu et al., 2001). We previously observed that CRMP-1 was downregulated in lung cancer tissue relative to normal tissue (Shih et al., 2001). Such findings suggest that CRMP-1 may be an invasion-suppressor gene (Steeg, 2001).

Because the CRMPs have overlapping spatial and temporal expression and their amino acid sequences are highly homologous, it is difficult to attribute a particular neuronal function to a specific CRMP. Thus, to resolve the functional roles of CRMP-1 *in vivo*, we disrupted the *CRMP-1* gene in mice and analyzed the phenotype of the CRMP-1 null (*CRMP-1*$^{-/-}$) mice.

Materials and Methods

Construction of targeting vectors. Mouse *CRMP-1* genomic DNA, 10 kb in length (nucleotides 32,963–42,541, according to the Celera Genomics database), coding for exons 3–6, was isolated from a 129/Sv genomic DNA BAC library (CITB mouse; Invitrogen, San Diego, CA) by the gap-repair technique (Lee et al., 2001) using the following primers: BACSP63′U (5′-CCAATTCCTCATGTTTGACAGCTTATCATCGAATTTCTGCCATTCATCCGCTTGCGGCCGCGATACGCGAGCGAACGTGA-3′) and CRMPBAC6D (5′-CTGAGCTATCAAATCTCCATTTTCTGCATGGACTAAGATCACAGCTCCCAAAGTCGACTTCTTAGACGTCAGGTGGCAG-3′). The 10 kb *CRMP-1* genomic DNA fragment was inserted into a pBR322 plasmid and further digested with appropriate restriction enzymes to obtain long and short arms for homologous recombination.

Two CRMP-1 targeting vectors were generated based on a pHPRT-loxP vector modified from pKO-loxP (Yadav et al., 2003) by replacing the neo cassette with the mouse hypoxanthine phosphoribosyltransferase (HPRT) gene. The pHPRT-loxP vector enables hypoxanthine, aminopterin, and thymidine (HAT) selection for the presence of HPRT under the control of the mouse PGK (phosphoglycerate kinase) promoter, as well as gancyclovir selection for absence of the viral TK (thymidine kinase) gene. The constructed targeting vectors I and II (see Fig. 1*A*) were used to insert the loxP-flanked HPRT into introns 5 and 3 of *CRMP-1*, respectively. The long and short CRMP-1 homologous arms derived from the 10 kb genomic DNA consisted of a 5.9 kb *Hin*dIII–*Apa*I fragment (nucleotides 35,089~41,010) containing a portion of intron 3, exons 4–5 and a portion of intron 5 of *CRMP-1* (long arm) and a 1.38 kb *Apa*I–*Nco*I fragment (nucleotides 41,010–42,390) containing the remaining portion of intron 5, 100 bp upstream of exon 6 of *CRMP-1* (short arm). The long and short arms were modified at their ends and inserted into the *Bam*HI and *Eco*RI sites of pHPRT-loxP, respectively. A third loxP sequence was obtained from pULwL (Kondo et al., 2003) and inserted at the blunt-ended *Cla*I site (nucleotide 36,967) of intron 3. Targeting vector II (see Fig. 1*A*) was derived from targeting vector I by shortening the long arm to a 1.9 kb *Hin*dIII–*Cla*I fragment (nucleotides 35,089~36,967) by deleting the *Xho*I fragment to become the short arm. The other arm in targeting vector II was the 4.0 kb *Xho*I to *Bam*HI fragment of targeting vector I (*Cla*I–*Apa*I fragment of nucleotides 36,967~41,010 of *CRMP-1*), blunt-ended and modified to have *Eco*RI ends before being inserted into the unique *Eco*RI site of pHPRT-loxP. There was a unique *Not*I site in pHPRT-loxP for linearization of both targeting vector I and II. The orientation and nucleotide sequences of the two constructs were confirmed by sequencing.

Selection and screening for homologous recombination and generation of homozygous CRMP-1$^{-/-}$ *mice.* Embryonic day 14 (E14) (E14TG2a, HPRT$^-$) embryonic stem (ES) cells were used for transfection experiments. Growth and expansion of the ES cells, ES cell DNA isolation, Southern blotting, and preparation of DNA probes by labeling with [α-^{32}P]dCTP were performed as described previously (Yu et al., 2004). The vector I-targeted ES clones (which failed to incorporate the third loxP site in intron 3) were subjected to Cre-mediated excision of the loxP-flanked HPRT fragment in intron 5. Cre excision was performed by transient transfection of the cells with a plasmid [pCAGGS-NLS-Cre; given by Dr. A. Nagy (Toronto University, Toronto, Ontario, Canada)] carrying the DNA coding for Cre recombinase (Vooijs et al., 2001). ES cells that survived the Cre transfection were subjected to limiting dilution and grown in the absence of HAT and then examined by Southern blotting for loss of HPRT. The resultant ES clones were further transfected by targeting vector II to recycle the loxP-flanked HPRT into intron 3. The Cre-recombinase plasmid was reintroduced to delete exons 4–5 of *CRMP-1*.

CRMP-1-deleted ES clones were injected into C57BL/6 blastocysts to establish chimeric mice. Germline transmission of the *CRMP-1*$^{-/-}$ allele was achieved by crossing the chimeric mice with normal C57BL/6 mice. Mice born from the intercross of the heterozygous F_1 littermates were used for most of the experiments. The littermates from the intercross of the heterozygous mice that had been backcrossed into the C57BL/6 background for four generations were also used in some experiments as specified.

Genotyping, Northern blot analysis, and reverse transcription-PCR. Mouse tail genomic DNA was isolated with a DNA Purification kit (Promega, Madison, WI). Genotyping of F_1 and successive progenies was performed on tail DNA by Southern blotting as described for ES cells (Yu et al., 2004), and by PCR using the following oligonucleotide primer pairs: primers 3U plus 3D and 4D or 4U plus 4D (see Fig. 1*A*) for the wild-type *CRMP-1* allele, and primers 3U plus 5D for the targeted allele. The primer sequences used were as follows: 3U, 5′-GCCAAATGACAGGCAGATTC-3′; 3D, 5′-ATTGATAGTGGGTCATGGGAG-3′; 4U, 5′-CAGCGCAGCAGAGCTCTTTCC-3′; 4D, 5′-ATGTGGAGATGGTAAAGTTCAAC-3′; and 5D, 5′-GCACAGTTCTACAGTAATAGCC-3′. The amplification reaction conditions were as follows: 94°C for 2 min, followed by 40 1 min cycles at 94°C, 60°C for 1 min, and 72°C for 1 min, followed by 72°C for 7 min.

For Northern blotting and reverse transcription (RT)-PCRs, whole brain and kidney were surgically removed from P7 wild-type and *CRMP-1*$^{-/-}$ mice, quickly frozen in liquid nitrogen, and stored at −80°C until used. RNA was isolated from the frozen samples by treating the homogenized thawed brain tissue specimens with TriPure (Genesis Biotech, Taipei, Taiwan). Northern blotting was performed using the glyoxal method as described previously (Yu et al., 2004). Briefly, a 25 μg aliquot of total RNA was electrophoresed and detected by a 1.2 kb *CRMP-1* cDNA fragment (coding for exons 1–11), and the glyceraldehyde-3-phosphate dehydrogenase (GAPDH) DNA fragment (Yu et al., 2004). Reverse transcription was performed using oligo-d(T)n as the primer for first-strand synthesis at 42°C (Yu et al., 2004), and the resultant product was used as the template for PCRs with oligonucleotide primers 2U (5′-AATGATGACCAGTCCTTCTAC-3′) plus 6D (5′-TCAAATCTCCATTTTCTGCATGG-3′) for *CRMP-1* message and specific primers for GAPDH (Yu et al., 2004). PCR conditions for all of the primer pairs were the same as described for tail DNA genotyping.

Western blotting. Samples of whole brains, cerebral cortex, hippocampus, and cerebellum of wild-type and mutant littermates at P1 and 8–12 weeks were homogenized in homogenization buffer [2 mM DTT, 5 mM EDTA, 2 μg/ml leupeptin, 2 μg/ml aprotinin, 10 μg/ml pepstatin, 1 mM TPCK (*N*-tosyl-L-phenylalanyl chloromethylketone), 50 mM NaF, 0.1 mM Na_3VO_4, 2.5 mM sodium pyrophosphate, and 1 mM

β-glycerophosphate in PBS]. Total protein concentrations were determined by Bio-Rad Protein Assay (Bio-Rad Laboratories, Hercules, CA). Equal amounts of total extracts were then analyzed by SDS-PAGE followed by immunoblotting and observation with enhanced chemiluminescence (Western; Millipore, Bedford, MA). The antibodies used were anti-CRMP-1 (prepared in-house or purchased from Millipore), anti-CRMP-2 (prepared in-house), anti-CRMP-4 (BD PharMingen, San Diego, CA), anti-growth-associated protein-43 (GAP-43) (Abcam, Cambridge, UK), and anti-microtubule-associated protein 2 (MAP2) and postsynaptic density-95 (PSD95) (Millipore) and anti-actin polyclonal antibodies (Sigma, St. Louis, MO). ECL data were semiquantified by densitometry using GenePix Pro 6.0 (Molecular Devices, Palo Alto, CA). The relative density of each band was normalized against that of α-actin and expressed as means ± SEM. Significant differences between groups were evaluated by applying Student's *t* tests; values of $p < 0.05$ were considered statistically significant.

Histology and DiI labeling. To demonstrate Nissl substance in tissue sections, mice at P7 were anesthetized by intraperitoneal injection of 400 mg/kg trichloroacetaldehyde (Kanto Chemical, Tokyo, Japan), and were perfused transcardially with normal saline followed by 4% paraformaldehyde in PBS. After fixation overnight at 4°C, the brains were removed, submerged in 30% sucrose overnight, and 15-μm-thick coronal sections were cut on a freezing microtome. Sections were stained with cresyl echt violet for 5 min, washed with distilled water, dehydrated in ethanol, and mounted onto glass slides. The hippocampal commissural projection in the brain was examined by labeling nerves with the lipophilic fluorescent dye 1,1′-dioctadecyl-3,3,3′,3′-tetramethyl-indocarbocyanine perchlorate (DiI) (Invitrogen) (Taniguchi et al., 1997). P1 neonatal mice used for DiI labeling analysis were perfused transcardially with 4% paraformaldehyde in PBS. After fixation, DiI crystals were injected into the CA3 region of the left hippocampus. The specimens were incubated at 37°C for 2 months, and 50-μm-thick brain sections were collected with a Vibratome (VT1000S; Leica, Nussloch, Germany). Sections were counterstained by submerging for 5 min in SYTOX Green nucleic acid stain (Invitrogen). After washing in distilled water, sections were mounted and observed under a fluorescence microscope (DMR; Leica).

Fluorescent immunohistochemistry. Mice (P1 and 8–12 weeks) were deeply anesthetized and perfused with normal saline followed by PBS with 15% picric acid, 4% paraformaldehyde, and 0.1% glutaldehyde. Whole brains were then isolated for postfixation overnight in the same fixative at 4°C and embedded in paraffin. Ten-micrometer-thick coronal sections were deparaffinized followed by epitope retrieval with citrate buffer. L1–L5 dorsal root ganglia (DRGs) were prepared without perfusion and sectioned as described above. After blocking with 5% fetal bovine serum (FBS) and 0.1% Triton X-100 in PBS (FBS/PBST), tissue sections were incubated overnight with individual primary antibodies against CRMP-1 (1:200 dilutions), MAP2 (1:200), GAP-43 (1:200), neurofilament (1:200), Tau-1 (1:50 or 1:200; recognizing dephospho tau) and PSD95 (1:200) (all from Millipore), Synapsin I (1:200; Calbiochem, La Jolla, CA) and Tau (1:200; recognizing unphosphorylated and phosphorylated tau proteins; Abcam) in FBS/PBST at 4°C. Unbound antibodies were removed by washing in PBST three times followed by detection with an Alexa Fluor 488 Signal-Amplification kit (Invitrogen) at room temperature for 1 h. After washing off unbound materials, sections were air-dried, coverslipped with mounting medium (DakoCytomation, Glostrup, Denmark), and examined on a confocal microscope (EZ-C1; Nikon, Tokyo, Japan). The computer software MetaMorph (Molecular Devices) was used to quantify the fluorescence intensity of the MAP2 labeling in confocal images of area CA1.

Electrophysiological recordings. Wild-type and mutant mice aged 8–12 weeks were killed by cervical dislocation, and their brains were quickly removed and placed in cold cutting buffer (87 mM NaCl, 2.5 mM KCl, 1.26 mM NaH_2PO_4, 25 mM $NaHCO_3$, 0.5 mM $CaCl_2$, 5.0 mM $MgSO_4$, 25 mM glucose, 75 mM sucrose, and 1 mM kynurenic acid) saturated with 95% O_2 and 5% CO_2. The hippocampus was sliced transversely into 400-μm-thick pieces and maintained for at least 1.5 h before recording in an interface chamber at room temperature where they were submerged in artificial CSF (aCSF) buffer (125 mM NaCl, 2.5 mM KCl, 1.26 mM NaH_2PO_4, 25 mM $NaHCO_3$, 2.0 mM $CaCl_2$, 1.0 mM $MgSO_4$, and 25 mM glucose) bubbled with 95% O_2 and 5% CO_2. A bipolar tungsten-stimulating electrode was placed in the middle of the striatum radiatum layer of area CA1, and extracellular field potentials were recorded using a glass microelectrode (3 MΩ; filled with aCSF). The pulse duration was 100 μs, and test responses were elicited at 0.05 Hz (GS-3200; Gould, Cleveland, OH). aCSF was perfused over the tissue continuously at a rate of 1–2 ml/min.

LTP was induced by two trains of 100 Hz stimulation, lasting 1 s for each train with a 20 s intertrain interval. The stimulation strength was set to provide field EPSPs (fEPSPs) with an amplitude that was 40~60% of the maximum. When paired-pulse facilitation (PPF) was examined in area CA1, paired-pulse stimulation was delivered at 0.01 Hz with interstimulus intervals (ISIs) of 20, 50, 80, 100, 200, 300, 400, and 500 ms with stainless-steel bipolar electrodes placed in the outer or inner molecular layers of the piriform cortex. fEPSPs from corresponding layers were recorded via glass pipettes filled with 3 M NaCl (resistance, 0.5–1 MΩ) and were amplified and filtered at 1 kHz. PPF ratio was calculated by dividing the amplitude of the second fEPSP by the amplitude of the first fEPSP.

Behavioral analysis. F_2 progeny of intercross matings between heterozygous F_1 mice, which have a mixed genetic background of 129/Ola and C57BL/6, were used for behavioral testing. Some experiments were repeated using mice that had been backcrossed into the C57BL/6 background for four generations. All behavioral results are presented as means ± SEM. Two-way ANOVAs were used to compare data among the groups. *Post hoc* Scheffé's tests were used to detect the sources of detected significant comparisons.

Water maze. Spatial memory performance was evaluated with the Morris water maze task (D'Hooge and De Deyn, 2001) using a circular water maze pool that was 120 cm in diameter and 60 cm high. The pool was divided into four quadrants and filled to a depth of 35 cm with milky water at 25 ± 0.5°C. A platform 9 cm in diameter was placed at the center of a fixed quadrant ~1.5 cm below the water surface. Young (8–12 weeks; backcrossed to C57BL/6 for four generations) and old (F_2 generation; 5–10 months) mice were placed in the testing room with the pool surrounded by visual cues external to the maze including three plain posters fixed on three walls. During training, mice were placed at equidistant positions along the edge of the four quadrants of the maze and allowed to search for the location of the submerged platform. The duration between entering the water and climbing onto the platform was recorded as the escape latency, and the mean latency for finding the invisible platform was calculated for each mouse. Each mouse received four consecutive daily training trials for 6 d. The movement paths of the mice were monitored and recorded with a video camera mounted on the ceiling over the maze, and subsequently analyzed by a software program (EthoVision; Noldus Information Technology, Wageningen, The Netherlands). When a mouse failed to find the platform within 60 s, it was picked up by the experimenter and placed onto the platform for the duration of the 20 s intertrial interval.

Retention was assessed with a probe trial given 24 h after the final training session. During the probe trial, the submerged platform was removed from the water maze and each mouse was placed in the water at the edge opposite to the quadrant where the platform had been located during the training trials. Mice were allowed to swim freely and search for the platform for 60 s. The duration that the mice searched within the quadrant that had previously contained the platform (target quadrant), and the durations spent in the other quadrants (nontarget quadrants) were recorded.

As a control for intact vision, the mice were subjected to a cued version of the water maze task 24 h after the probe trial. In the cued task, mice were placed in the water maze with the platform mounted 1 cm above the milky water surface so that it was visible. The escape latency of each mouse was determined.

Locomotor activity. Spontaneous locomotor activity was assessed by placing each mouse in a small dark area (448 × 448 × 450 mm) that served as an activity chamber. They were allowed to explore the environment for 1 h. Total distance traveled, time and distance in the center of the field, and time and distance in the perimeter of the field were calcu-

lated by a computer that was connected to the activity chamber (TSE Technical & Scientific Equipment, Bad Homburg, Germany).

Nociception tests. The tail-flick and hot-plate analgesia tests were performed according to protocols described by Eddy and Leimbach (1953). For the former, each mouse was gently restrained in a small plastic cylinder so that its tail was placed above an apparatus with a radiant heat source connected to an automatic timer to assess the analgesic response (IITC Life Science, Woodland Hills, CA). The heat source was set at an arbitrary setting of "55." The latency of the mouse to flick its tail away from the heat source was recorded. A cutoff latency of 50 s was adopted to avoid tissue damage. The hot-plate test was performed on mice kept in a glass cylinder (17 cm high by 16 cm diameter) on a heated hot-plate surface (Fargo Instruments, Fargo, ND) set at 55 ± 0.5°C. A positive response was recorded when the mouse rubbed its forepaws together, wiggled its hindpaws, or jumped away from the plate. A cutoff time of 60 s was used.

Results

Generation of *CRMP-1*$^{-/-}$ mice

Figure 1*A* summarizes the strategy used to delete exons 4–5 from the mouse *CRMP-1* gene. A loxP-flanked HPRT cassette was initially homologously recombined into intron 5 using targeting vector I. The targeted allele ("t") was identified as a 10.8 kb *Afl*II fragment compared with an 8.3 kb wild-type allele ("+") by Southern blot hybridization with 5′ "probe A" (Fig. 1*B*, lanes 1 and 2). The same bands were also labeled with the 3′ probe (probe B) (data not shown). The efficiency for the "t" allele was 6 of 116. Of the six clones, none incorporated the third loxP site in intron 3. These clones were therefore transfected with a plasmid transiently expressing Cre recombinase to excise the HPRT maker, identified by Southern blotting, and then transfected again with targeting vector II. The resultant ES cell clones were screened for the ineffective (lane 4) and effective incorporation of the loxP-flanked HPRT into intron 3 (*cis*-event). The desired allele ("fl") was identified by the presence of a 9.8 kb *Afl*II–*Bam*HI band or a 10.8 kb *Afl*II band (Fig. 1*B*, lanes 3 and 7, respectively). When the HPRT marker was inserted into the wild-type chromosome (*trans*-event), the ES clone showed a 10.7 kb *Afl*II–*Bam*HI band and a 6.8 kb loxP allele (lane 5). The targeting efficiencies were 15 of 456 and 13 of 456 for the *cis*- and *trans*-events, respectively. Deletion of *CRMP-1* by Cre excision of exons 4–5 generated a 4.3 kb *Afl*II band plus the wild-type 8.3 kb allele (lane 6). The *CRMP-1*-deleted ES cell clone (lane 6) was used to generate chimeric mice, which transmitted the deleted *CRMP-1* allele to their offspring showing a genotype of 8.3 and 4.3 kb *Afl*II bands for the wild-type and KO allele, respectively (Fig. 1*C*). Southern blot analysis was also used to confirm the absence of any Cre DNA integration in the mouse genomes (data not shown).

Verification of a null allele for CRMP-1

Northern blotting demonstrated successful deletion of full-length 2.7 kb *CRMP-1* mRNA (Fig. 1*D*), and RT-PCR showed the lack of a 582 bp RT-PCR product in the *CRMP-1*$^{-/-}$ mice (Fig. 1*E*). These results confirmed CRMP-1-null status in the knock-out progeny. We detected a shorter RT-PCR band, 356 bp in length, in the heterozygous (+/−) and homozygous mice. Sequencing of the products revealed that the 582 bp band represents the correctly spliced RNA of exons 3–4 with the authentic *CRMP-1* reading frame. The 356 bp product results from the splicing of exon 3 to exon 6, which generates a termination codon near the splicing junction following amino acid residue 106 (data not shown). The absence of CRMP-1 protein in the mutants was confirmed by Western blot analysis (Fig. 1*F*). A major band near 62 kDa, the predicted size for mouse CRMP-1, was detected in wild-type and heterozygous (*CRMP-1*$^{+/-}$) mice, but not in homozygous mice. These results indicate that we successfully generated a *CRMP-1* knock-out mouse line.

CRMP-1$^{-/-}$ mice were viable and fertile

Of 249 F_2 progeny born from intercrosses between heterozygous mice, about an equal number of male and female offspring survived beyond weaning. The Mendelian ratio was 59:128:62 for wild-type to heterozygous to homozygous mice. *CRMP-1*$^{-/-}$ mice developed normally and exhibited no gross abnormalities in size, body weight, or anatomical features of major organs at young or old ages (>12 months) (data not shown). Blood metabolic profile, including blood sugar, liver enzymes, blood urea nitrogen, creatinine, and electrolytes of *CRMP-1*$^{-/-}$ mice did not differ from that of their wild-type littermates (data not shown). Expression of the other members of the CRMP family, such as CRMP-2 and CRMP-4, did not differ between wild-type and *CRMP-1*$^{-/-}$ mice (Fig. 1*F*), indicating that the grossly normal phenotype of homozygous mutant mice was not an effect of compensatory CRMP-2 and/or CRMP-4 overexpression.

Analysis of postnatal mouse brains organization

Examination of forebrain sections by Nissl staining showed no distinguishing abnormalities in the *CRMP-1*$^{-/-}$ mice. The pyramidal cell layer and dentate gyrus (DG) regions of the hippocampus from *CRMP-1*$^{-/-}$ brains at P7 were indistinguishable from those of wild-type littermates in terms of size, shape, and gross anatomy (Fig. 2*A*). The development and organization of the neuronal fibers in the corpus callosum of the *CRMP-1*$^{-/-}$ brain at P1 were comparable with those of wild-type littermates (Fig. 2*B*). Furthermore, immunoreactivity of several neuronal markers, such as MAP2, GAP-43, Tau, and neurofilament (data not shown), did not differ between wild-type and *CRMP-1*$^{-/-}$ mouse brains at P1. The above observations together indicate that CRMP-1 does not play an essential role in prenatal or postnatal mouse brain development.

Expression of CRMP-1 in the adult mouse brain of wild-type but not *CRMP*$^{-/-}$ mice

Adult mouse brains were analyzed for CRMP-1 protein expression. As shown in Figure 3*A*, CRMP-1 immunoreactivity was evident in the cortex, the hippocampus (predominantly CA1 and CA3 pyramidal cells), and cerebellar Purkinje cells (arrow) in wild-type mice. This labeling pattern was not present in the homozygous specimens, an observation consistent with the loss of CRMP-1 in the knock-out mice. A preliminary estimation by Western blotting and densitometry indicated that a higher level of CRMP-1 was detected in the hippocampus than in the cortex or cerebellum of the adult wild-type mouse brain (Fig. 3*B*). We thus focused our examination of the adult homozygous mutant mouse brains primarily on the hippocampus.

Altered configuration of area CA1 in adult *CRMP-1*$^{-/-}$ mice

In the adult brain, strong CRMP-1 labeling was observed in the somata of CA1 and CA3 pyramidal cells (Fig. 3), whereas very weak labeling was observed in the axons. This observation was consistent with the previous results using a different CRMP-1 antibody, except that CRMP-1 was previously also detected in the dendrites of CA1 pyramidal cells (Bretin et al., 2005).

To examine the influence of loss of CRMP-1 on the organic structure of the adult mouse brain, which might be distinct from that of the neonatal one, we used several neuronal structure specific markers. As shown in Figure 4, the apical dendrites of CA1

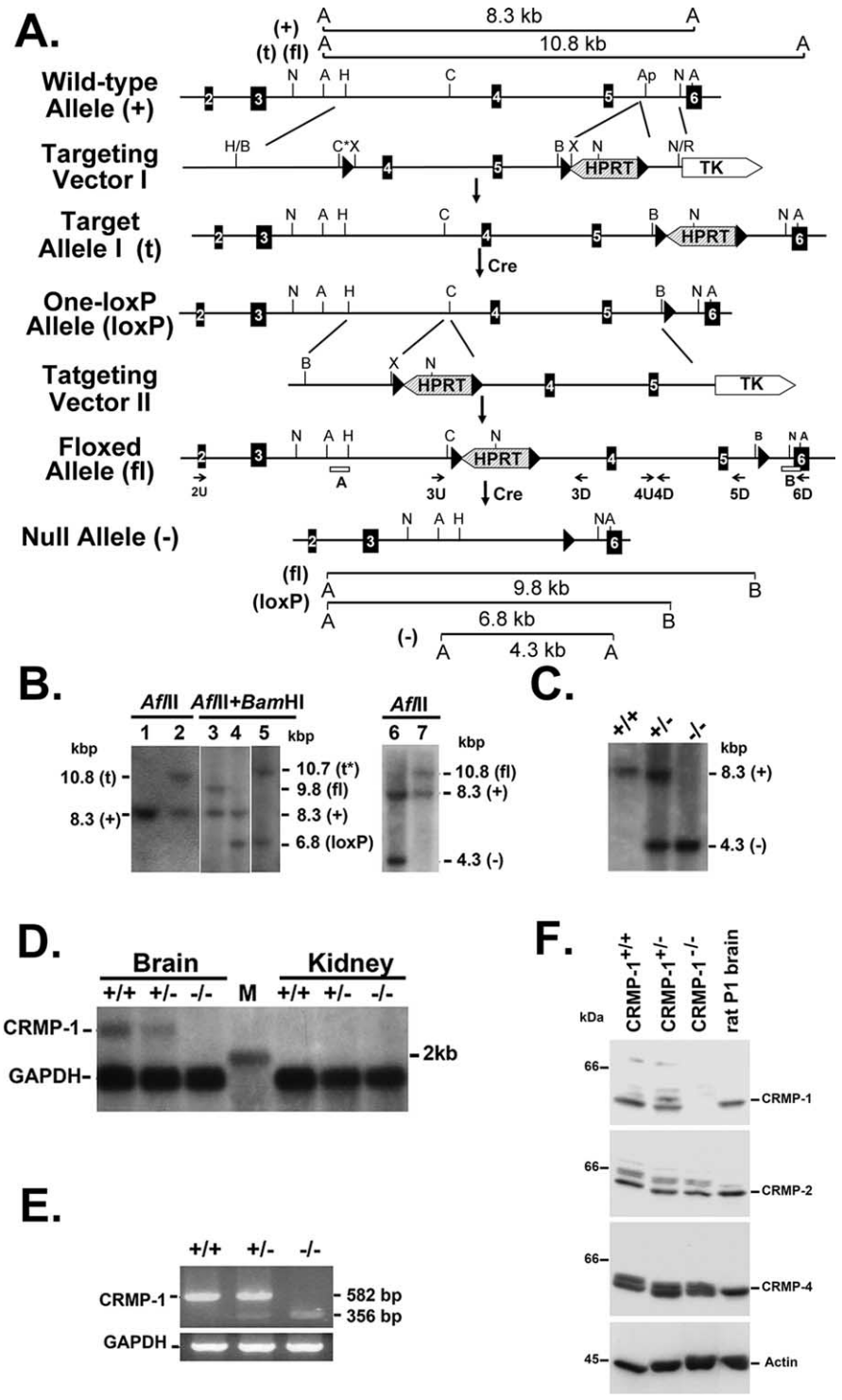

Figure 1. Generation and characterization of *CRMP-1*$^{-/-}$ mice. ***A***, The genomic structure of *CRMP-1* and the targeted alleles. The *CRMP-1* exons 2–6 (filled boxes) are depicted along with restriction enzyme sites (A, *Afl*II; Ap, *Apa*I; B, *Bam*HI; C, *Cla*I; H, *Hin*dIII; N, *Nco*I; X, *Xho*I; R, *Eco*RI). The wild-type allele (+) targeted by vector I generated the allele ("t") harboring a loxP (filled triangle)-flanked *HPRT* (hatched box) in intron 5. Cre excision generated the one-loxP allele. Subsequent transfection of the one-loxP-containing ES cells with vector II generated the floxed allele (fl). Subsequent excision by Cre deleted the *HPRT* and exons 4 and 5 [the null allele (−)]. Open bars, Probes A and B for Southern blotting. Primers (2U, 3U, 3D, 4U, 4D, 5D, and 6D) for genotyping by PCR. C* in vector I, Deleted *Cla*I site. ***B***, Southern blotting of recombinant ES cell clones digested by *Afl*II and *Afl*II plus *Bam*HI and detected by probes A and B. DNA in each lane, 5–10 μg. Only probe A results are shown. Lane 1, Wild-type ES cells (showing 8.3 kb "+" allele). Wild-type allele is omitted in the following descriptions. Lane 2, Vector I targeted clone (10.8 kb; "t" allele). Lanes 3–5, DNA from ES cells of lane 2 after cre-excision and successful vector II recombination (lane 3, 9.8 kb floxed "fl" allele), unsuccessful vector II recombination in *cis* (lane 4, 6.8 kb "loxP" allele), and successful vector II recombination in *trans* (lane 5, a loxP allele plus a t* allele denoting the clone with the loxP-flanked HPRT fragment in intron 3 of the wild-type allele of lane 4). Lane 6, ES cell clone in lane 7 after Cre transfection to generate the *CRMP-1*$^{-/-}$ allele, the (−) allele. Lane 7, ES cell clone in lane 3 by *Afl*II. ***C***, Southern blotting of *Afl*II-digested tail DNA from pups derived from ES cell clones of lane 6 of panel B. +/+, +/−, and −/−, Wild-type, heterozygous, and homozygous *CRMP-1*$^{-/-}$ mice. Both probes A and B gave the same pattern. ***D***, Northern blotting of 20 μg of total RNA from P7 mouse brains and kidneys, using exons 1–11 CRMP-1 cDNA and a *GAPDH* probe. M, RNA size maker (MBI Fermentas, Hanover, MD). ***E***, RT-PCR analysis. Total RNA (P7) of brains and PCR primers 2U and 6D were used. The 582 and 356 bp bands represent the wild-type and knock-out alleles, respectively. ***F***, Western blot analysis of CRMPs in whole-brain extracts from *CRMP-1*$^{+/+}$ and *CRMP-1*$^{-/-}$ mice at P1. Tissue extract samples (15 μg) were loaded in each lane. The membrane was first reacted with anti-CRMP-1 antibody (in-house), followed by anti-CRMP-2, anti-CRMP-4, and then anti-actin antibodies (internal control) with stripping and washing steps in between each antibody reaction. Rat P1 brain, Positive control. Lanes +/+, +/−, and −/−, Wild-type, heterozygous, and homozygous *CRMP*-1 knock-out mice, respectively. Multiple CRMP bands were attributable to phosphorylation events.

pyramidal neurons of adult *CRMP-1*$^{-/-}$ mice exhibited altered expression of the dendritically localized protein MAP2. Specifically, the MAP2-positive neurites of *CRMP-1*$^{-/-}$ mice were shrunken (Fig. 4*a–c*), with the labeling localized mainly near the proximal portion of the apical dendrites, making the MAP2 dendritic labeling at the distal portion less salient and disorganized in the knock-outs than in the wild-type mice (Fig. 4*A–C*). Our computer software-estimated averages of MAP2 fluorescence levels revealed that the proximal and distal portions of the dendrites had nearly equal values (distal divided by proximal, 1.07 ± 0.08; $n = 3$ brain slices). In contrast, MAP2 fluorescence of the distal portion of the dendrites was only 87% of that in the proximal portion. Double labeling of area CA1 with MAP2 and the microtubule-associated protein Tau (staining for phosphorylated and unphosphorylated tau proteins) did not reveal colocalization patterns (data not shown). These findings suggest that area CA1 dendrites were not properly formed in CRMP-1$^{-/-}$ mice and that this malformation was not related to abnormal Tau expression.

Adult *CRMP-1*$^{-/-}$ mice had reduced expression of the postsynaptic density marker PSD95 in the distal portion of the dendrites of CA1 pyramidal cells (Fig. 4*f*) relative to their wild-type littermates (Fig. 4*F*). In contrast, PSD95 immunoreactivity in the proximal dendrites of CA1 pyramidal cells was indistinguishable between mutant (Fig. 4*e*) and wild-type (Fig. 4*E*) mice. Immunolabeling of GAP-43, a plasticity-related protein and growth cone marker, revealed similar features. There

were fewer growth cones in the dendritic layer of CA1 of *CRMP-1*$^{-/-}$ brains (Fig. 4*i*) than in wild-type controls (Fig. 4*I*), although the pyramidale and stratum oriens layers was indistinguishable between mutant and wild-type mice (Fig. 4*h*,*H*, respectively). Double immunolabeling did not reveal clear colocalization of GAP-43 and synapsin I. These results indicate that both dendrites and dendritic spine are poorly formed in the *CRMP-1*$^{-/-}$ mice. As shown in Figure 5*A*, double immunolabeling for Tau-1 and synapsin I did not reveal any visible differences between *CRMP-1*$^{-/-}$ and wild-type mice in the expression of these axonal markers in CA1, CA3, or DG, indicating that the knock-out did not alter axon formation.

Decreased GAP-43 and PSD95 expression in the *CRMP-1*$^{-/-}$ hippocampus

Because MAP2, PSD95, and GAP-43 labeling patterns were altered in area CA1 of *CRMP-1*$^{-/-}$ knock-out mice, we conducted Western blot analyses to provide a quantitative assessment of these effects. As shown in Figure 5*B*, GAP-43 protein levels in the hippocampus, but not cortex or cerebellum, of *CRMP-1*$^{-/-}$ mice were decreased (Fig. 5*B*,*C*) ($p < 0.001$ vs wild-type mice; $n = 3$ per group). Meanwhile, MAP2 and synapsin I protein levels in the cortex, hippocampus, and cerebellum of *CRMP-1*$^{-/-}$ mice did not differ from those in wild-type controls. Interestingly, PSD95 protein levels were also decreased in the hippocampus of *CRMP-1*$^{-/-}$ mice ($p < 0.05$ vs wild-type mice; $n = 3$ per group).

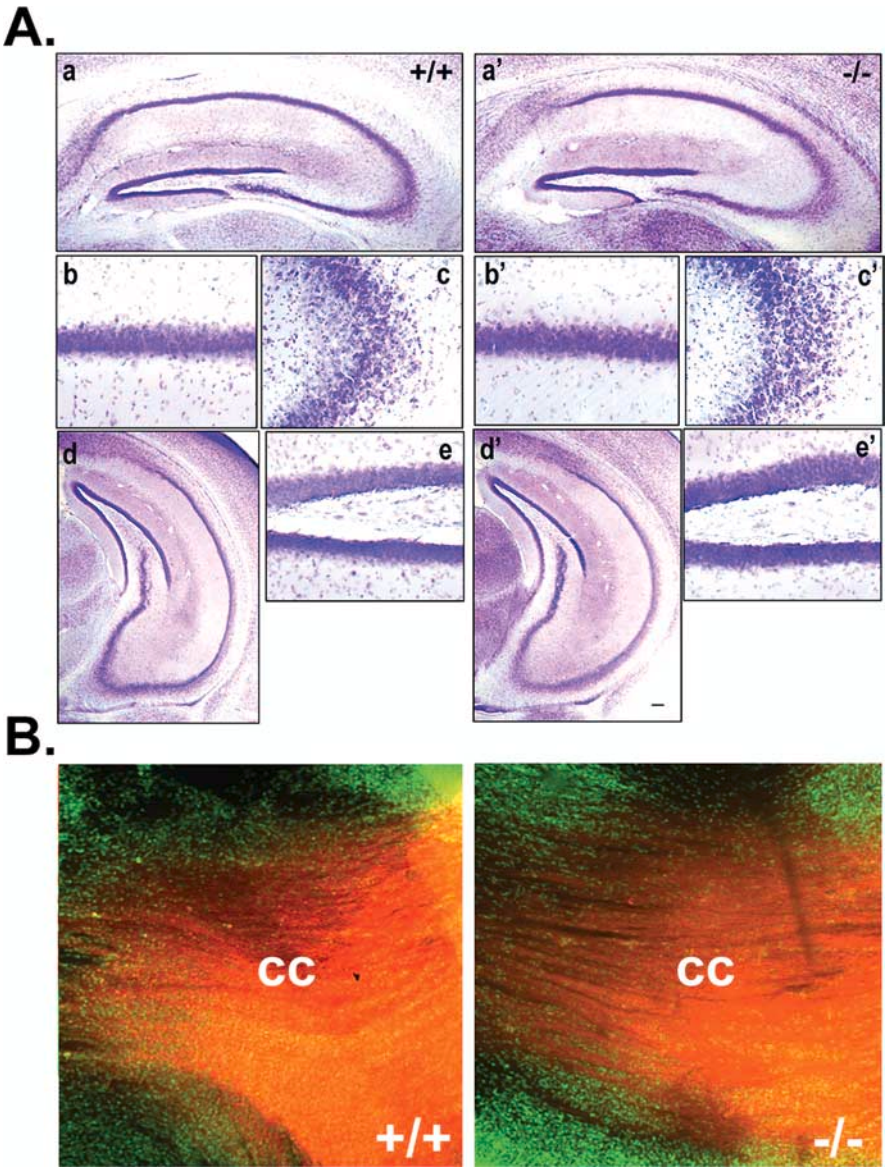

Figure 2. Histology and neural morphology of *CRMP-1*$^{+/+}$ and *CRMP-1*$^{-/-}$ mice. ***A***, Cresyl violet staining of the hippocampus of wild-type *CRMP-1*$^{+/+}$ (+/+; ***a–e***) and *CRMP-1*$^{-/-}$ (−/−; ***a′–e′***) brains at P7. No difference between wild-type and knock-out brains was observed at low (dorsal, ***a*** vs ***a′***; ventral, ***d*** vs ***d′***) or high magnification in any of the subregions of hippocampus [CA1 (***b***, ***b′***), A3 (***c***, ***c′***), and DG (***e***, ***e′***)]. ***B***, Comparisons of DiI tracing were conducted in P1 of *CRMP-1*$^{+/+}$ (left) and *CRMP-1*$^{-/-}$ (right) mice using fluorescence microscopy. DiI crystals were placed in CA3, and the contralateral hippocampus was analyzed. Nuclei were counterstained with SYTOX Green. cc, Corpus callosum.

LTP induction, but not PPF, in area CA1 was impaired in *CRMP-1*$^{-/-}$ and *CRMP-1*$^{+/-}$ mice

To dissect the functional consequences of the abnormal CA1 structure in homozygous mutant mice, we examined LTP between the Schaffer collaterals and principal CA1 pyramidal neurons in hippocampal slices prepared from *CRMP-1*$^{-/-}$ mice and their wild-type and heterozygous littermates. As shown in Figure 6*A*, tetanic stimulation of the Schaffer collaterals resulted in robust LTP in slices from wild-type mice. However, both *CRMP-1*$^{-/-}$ and *CRMP-1*$^{+/-}$ slices had impaired LTP maintenance 60 min after LTP induction ($p < 0.05$, unpaired Student's *t* test). Sensitivity to loss of a single allele of *CRMP-1* as well as to the full null genotype suggests that normal CRMP-1 expression is required for normal LTP induction.

To further study the possible source of LTP impairment in the mutant mice, we examined PPF of fEPSPs. As shown in Figure 6*B*, there was no significant difference in the PPF profiles of slices from any of the three genotypes. With a 40 ms interpulse interval, the ratio of the slope of the second to first fEPSP was 1.70 ± 0.09 (13 slices from 5 mice), 1.44 ± 0.10 (13 slices from 7 mice), and 1.53 ± 0.21 (13 slices from 5 mice) in *CRMP-1*$^{+/+}$, *CRMP-1*$^{+/-}$, and *CRMP-1*$^{-/-}$ mice, respectively (Fig. 6*B*).

CRMP-1$^{-/-}$ mice demonstrated impaired performance in the Morris water maze

We examined acquisition and retention performance in the Morris water maze task, a hippocampus-dependent spatial task, in young adult (8–12 weeks) and older adult (5–10 months) wild-type and *CRMP*$^{-/-}$ mice. Both the wild-type and the knock-out young adult mice learned to navigate to the platform over the course of 6 training days, as indicated by the progressive decrease in escape latencies (Fig. 7*A*). However, *CRMP-1*$^{-/-}$ mice consistently had longer mean daily escape latencies than their wild-type littermates. Although all mice learned to locate the position of the submerged platform, *CRMP-1*$^{-/-}$ mice showed a different learn-

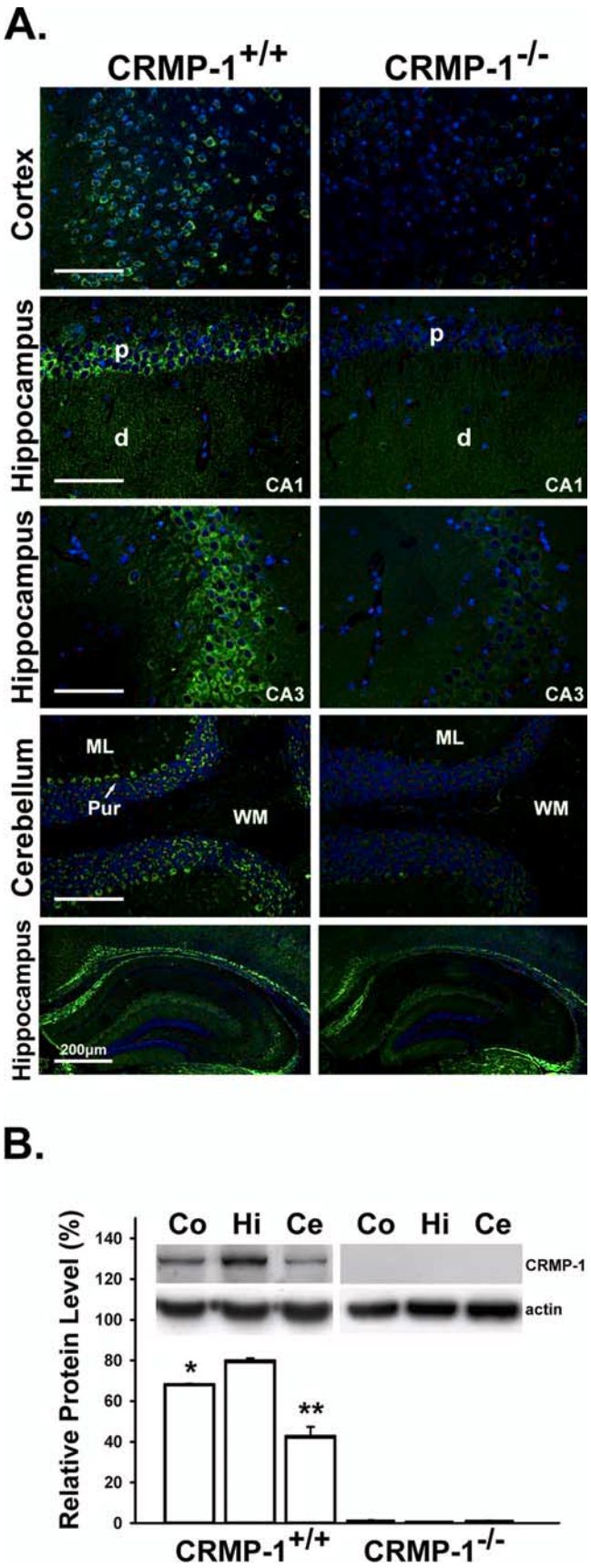

Figure 3. CRMP-1 expression in adult *CRMP-1*$^{+/+}$ and *CRMP-1*$^{-/-}$ mouse brains. ***A***, Paraffin-embedded sections from *CRMP-1*$^{+/+}$ and *CRMP-1*$^{-/-}$ mice (8–12 weeks of age) were labeled with anti-CRMP-1 (green) followed by DAPI (4′,6′-diamidino-2-phenylindole) nuclear counterstain (blue) and analyzed by confocal microscopy. CRMP-1 was identified predominantly in hippocampal CA1 pyramidal cells and Purkinje cells (arrow) in the cerebellum. Positive neurofilament labeling (green) of serial sections served as a validation of the appropriateness of the *CRMP-1*$^{-/-}$ brain samples. Co, Cortex; Hi, hippocampus; Ce, cerebellum; p, pyramidal cell layer; d, apical dendritic layer; ML, molecular layer; WM, white matter; Pur, Purkinje cell. Scale bar, 50 μm (unless otherwise specified). Neurofilament labeling, which served as a positive control, was indistinguishable between the two genotypes. ***B***, Semiquantitative Western blot analysis. Total protein extracts of cortex, hippocampus, and cerebellum from three 8- to 12-week-old mice were immunoblotted with anti-CRMP-1 polyclonal antibody. Relative protein levels (% α-actin) were quantified by densitometer scanning and normalized to corresponding α-actin loading controls. Results are presented as mean ± SEM. *$p < 0.01$ versus wild-type hippocampus; **$p < 0.005$ versus wild-type hippocampus.

ing pattern from that of wild-type littermates [day ($F_{(5,170)} = 19.970$; $p < 0.001$) and genotype ($F_{(1,34)} = 8.152$; $p < 0.01$)].

The older adult wild-type and *CRMP*$^{-/-}$ mice both learned to navigate to the platform over the course of 5 training days as indicated by the progressive decrease in escape latencies (Fig. 7*B*) (escape latency: day, $F_{(4,72)} = 13.72$, $p < 0.001$). However, there was a significant difference between the escape latencies of the two genotypes ($F_{(1,18)} = 5.02$; $p < 0.05$). Wild-type mice reached the platform faster than the *CRMP*$^{-/-}$ mice on day 2 (34.9 vs 52.9 s; $p < 0.05$; two-way ANOVA followed by *post hoc* Scheffé's test). Both wild-type and *CRMP-1*$^{-/-}$ mice could locate the platform during the cued test, indicating that there were no visual deficits in the knock-out mice (Fig. 7*B*).

During the probe trial, the young adult wild-type mice spent more time in the target quadrant than in the nontarget quadrants ($p < 0.005$), whereas the young adult *CRMP-1*$^{-/-}$ mice did not (Fig. 7*C*). In the aged groups (Fig. 7*D*), wild-type animals spent much more time in the target quadrant than their *CRMP-1*$^{-/-}$ littermates (Fig. 7*D*) ($p < 0.0001$). These knock-out performance deficits in the probe test are consistent with an impairment of hippocampal-dependent memory in the *CRMP-1*$^{-/-}$ mice. Curiously, *CRMP-1*$^{-/-}$ mice spent more time in the nontarget quadrants than in the target quadrant; the explanation for this observation is not clear.

Spontaneous locomotor activity did not differ between *CRMP-1*$^{-/-}$ and wild-type littermates in either age cohort. Thus, the impaired escape latency of the *CRMP-1*$^{-/-}$ mice cannot be attributed to any generalized motor deficits. Likewise, *CRMP-1*$^{-/-}$ mice did not differ from wild-type controls in the hot-plate ($n = 8\sim10$ per group) or tail-flick tests ($n = 9\sim10$; $p > 0.05$) (data not shown).

Discussion

Establishment of *CRMP-1*$^{-/-}$ mouse line

We generated *CRMP-1*$^{-/-}$ mice to elucidate the *in vivo* function of CRMP-1. Two vector constructs were used because the initial recombination event was inefficient and only the loxP-flanked HPRT cassette in intron 5, but not the unique loxP at intron 3, was incorporated into the chromosome. Although the homologous arms flanking the unique loxP fragment appeared to be too short to assure successful recombination (Fig. 1*A*), the targeted ES cells were germline competent. Homozygous *CRMP-1*$^{-/-}$ mice did not exhibit infertility or gross abnormalities, indicating that CRMP-1 is not essential for embryogenesis, reproduction, and growth.

The *CRMP-1*$^{-/-}$ transcript

We detected a shorter transcript encoding only the first 106 aa of CRMP-1 in the mutants (Fig. 1*E*). Our inability to detect the truncated peptide by either of two anti-CRMP-1 antibodies (Fig. 1*F*) (data not shown), suggests that it was either not translated or

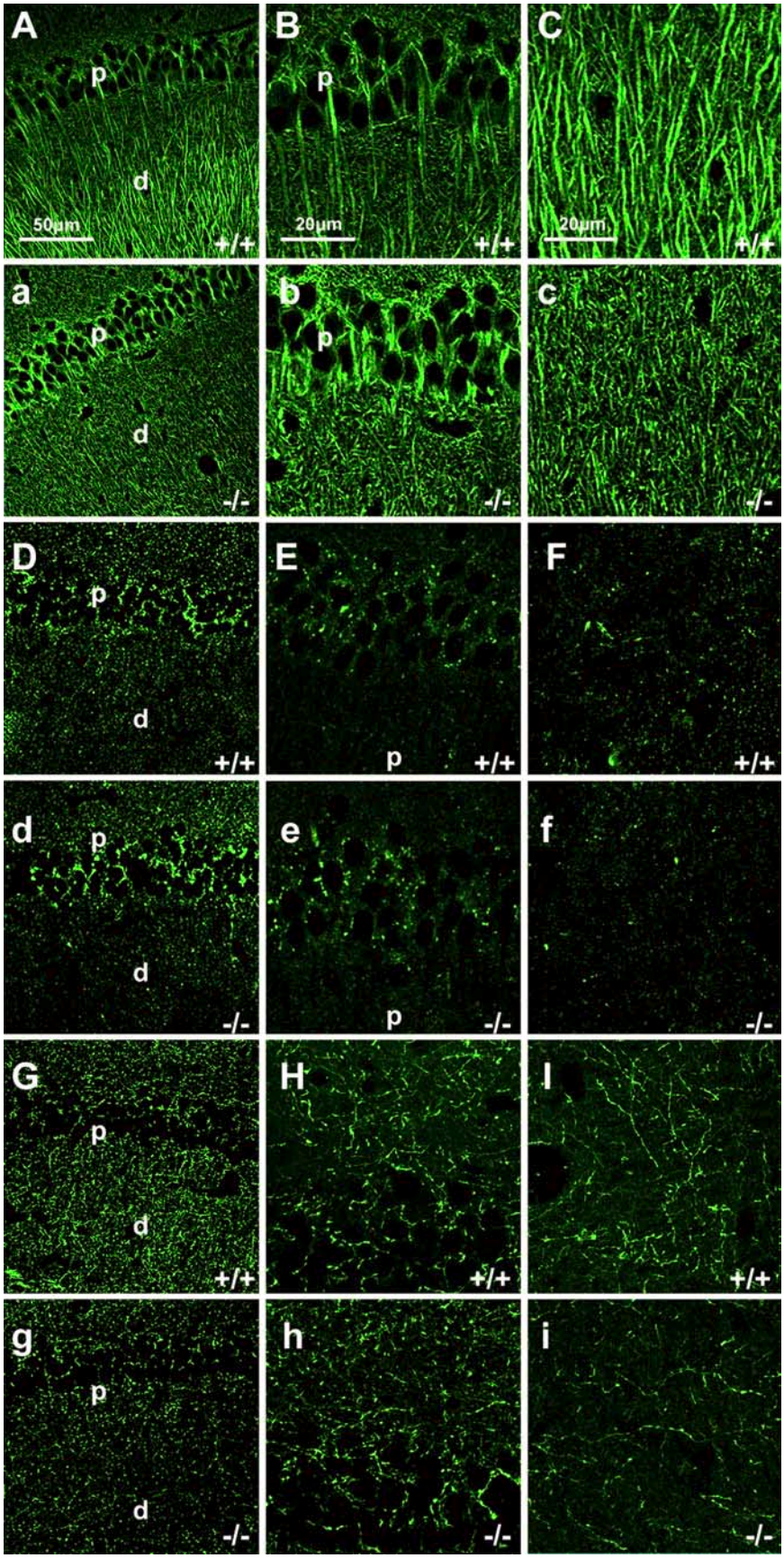

Figure 4. Distribution of neuronal markers in and organization of the hippocampal region of the wild-type (***A–I***) and *CRMP-1*$^{-/-}$ (***a–i***) mice. Representative images from the analysis of several mice are shown (8–12 weeks; $n = 3$ and 4 for wild-type and knock-out mice, respectively). Confocal microscopy images of MAP2 (***A–C***, ***a–c***); PSD95, postsynaptic density specific marker (***D–F***, ***d–f***); and GAP-43 (***G–I***, ***g–i***) immunoreactivity in area CA1. Higher magnification of the stratum pyramidal (***B***, ***b***, ***E***, ***e***, ***H***, ***h***) and stratum radiatum (***C***, ***c***, ***F***, ***f***, ***I***, ***i***) of the CA1 area were shown in parallel for the respective lower magnification (***A***, ***a***, ***D***, ***d***, ***G***, ***g***). Low magnifications were generated from projections of 8 serial optical 1.05 μm sections and higher magnifications were 22 optical 0.3 μm sections. The arbitrary MAP2 fluorescence levels in the proximal and distal portions of the dendrites were quantified by the MetaMorph software (Molecular Devices) and expressed as relative values by normalization to value of the proximal part. The MAP2 intensity (distal/proximal part of the dendrite) in *CRMP-1*$^{-/-}$ (0.87 ± 0.03; $n = 4$) and wild-type (1.07 ± 0.08; $n = 3$) sections differed ($p = 0.019$). p, Pyramidal layer; d, apical dendritic layer.

degraded instantaneously on translation. It is doubtful that the truncated peptide, even if present, could compensate for the full-length CRMP-1 for several reasons. First, several important phosphorylation sites (e.g., Ser522, Ser518, and Thr509) (Gu et al., 2000; Brown et al., 2004; Uchida et al., 2005; Cole et al., 2006) are not included in the truncated peptide. Furthermore, CRMPs function as oligomers, and hetero-oligomerization between the CRMPs is favored. The truncated peptide lacks the oligomerization sites at residues 281–435 (Wang and Strittmatter, 1997), 367–368, and 487–489 (Deo et al., 2004). If translated, however, the truncated protein would include the regions within residues 8–134 (Wang and Strittmatter, 1997; Deo et al., 2004) and 49–56 (Deo et al., 2004), which have been proposed to be functionally important (Wang and Strittmatter, 1997). Thus, although the lack of the functional regions described above would preclude the truncated peptide from compensating functionally for the full-length protein, it is possible that it could act as a dominant-negative variant if the putative functional regions that are preserved bind ligands.

The *CRMP-1*$^{-/-}$ mouse phenotype: hippocampus-specific neuronal, physiological, and behavioral defects

The absence of organic structural abnormality in neonatal mutant mouse brains suggests that the CRMPs may have redundant roles during embryogenesis. Consistent with a previous description (Bretin et al., 2005), we observed that CRMP-1 was expressed in the adult cortex, hippocampal CA1 and CA3 regions, and cerebellum. However, we did not replicate Bretin et al.'s observation of CRMP-1 in CA1 pyramidal cell dendrites. This could be attributable to differences in antibody specificity or avidity. We found that MAP2 immunoreactivity in adult knock-outs was localized disproportionately in the

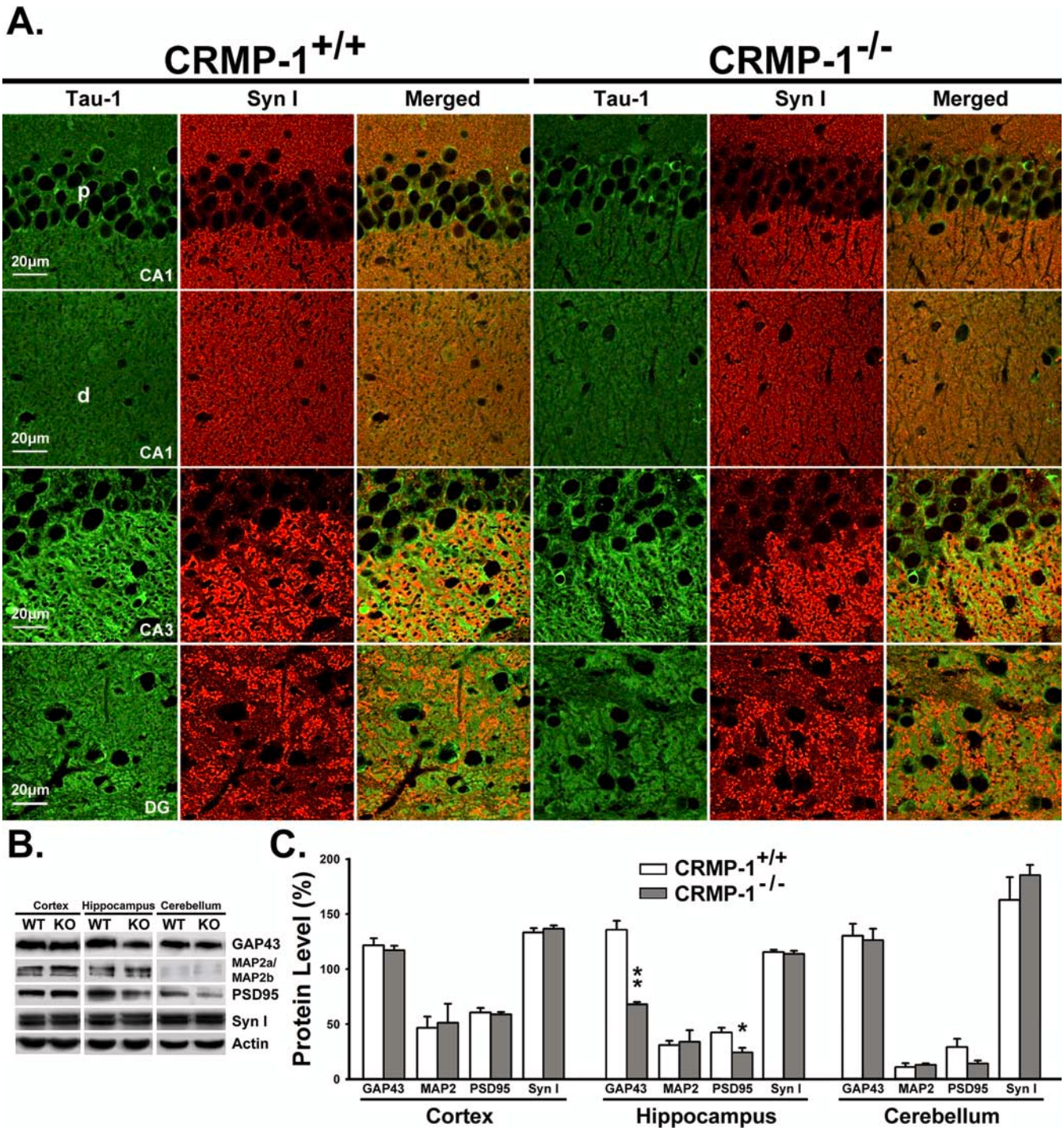

Figure 5. Double immunohistochemical examination of axon formation (***A***) and Western blotting of GAP-43, MAP2, PSD95, and synapsin I levels in wild-type and *CRMP-1* $^{-/-}$ mouse brain regions (***B***, ***C***). ***A***, Wild-type and mutant mouse hippocampal sections were incubated with anti-Tau-1 (1:50 dilution; Millipore; MAB3420) and anti-synapsin I (1:50; Calbiochem; 574777) antibodies to reveal axonal cytoarchitecture. FITC-conjugated goat anti-mouse IgG (1:500) and rhodamine-conjugated goat anti-rabbit IgG (1:500) secondary antibodies were used to reveal Tau-1 and synapsin I, respectively. Double channel images were captured by confocal microscope (Nikon EZ-C1) of a single optical (0.3 μm) section. ***B***, Representative patterns of Western blot analysis showing GAP-43, MAP2 (MAP2a and MAP2b), PSD95, synapsin I, and actin protein levels in isolated cerebral cortex, hippocampus, and cerebellum. ***C***, Quantification of MAP2, GAP-43, PSD95, and synapsin I protein levels in ***B*** were normalized to α-actin ($n = 3$ per genotype). Data are presented as means ± SEM. *$p < 0.05$; **$p < 0.001$. +/+, Wild-type mice; −/−, *CRMP-1* $^{-/-}$ mice. p, Pyramidal layer; d, apical dendritic layer; WT, wild type; KO, knock-out.

proximal portion of CA1 dendrites (Fig. 4*a–c*), indicating that CA1 dendrites were not properly formed. This finding suggests that CRMP-1 is important for CA1 pyramidal cell neurite formation. Whether this can be substantiated by findings that CRMP-1 participates in neurotrophin-induced neurite formation/extension of DRGs (Quach et al., 2004) is not clear.

Alternatively, because CRMP-1 has been shown to colocalize with MAP2 in CA1 pyramidal cell dendrites (Bretin et al., 2005), it may be that dendrite elongation was actually affected by MAP2 (Harada et al., 2002), the expression of which may have been altered by the absence of CRMP-1. Although the mechanism for such an interaction is far from clear, one may speculate that be-

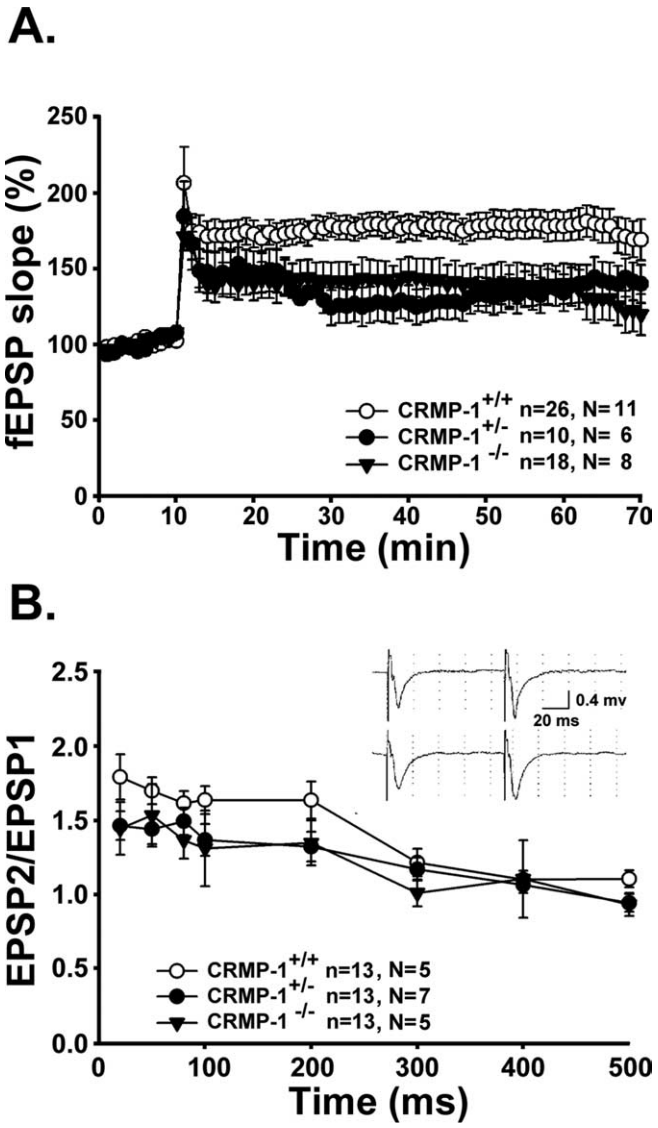

Figure 6. Attenuated LTP in area CA1 of *CRMP-1*$^{+/-}$ and *CRMP-1*$^{-/-}$ mice. ***A***, Strong tetanus stimulation (twice at 100 Hz for 1 s each separated by 20 s) in the stratum radiatum layer of CA1 induced LTP. Note that induction and maintenance of LTP was inhibited in *CRMP-1*$^{+/-}$ and *CRMP-1*$^{-/-}$ mice. Data are presented as means ± SEM (*CRMP-1*$^{+/+}$, $n = 26$ from 11 mice; *CRMP-1*$^{+/-}$, $n = 10$ from 6 mice; *CRMP-1*$^{-/-}$, $n = 18$ from 8 mice). ***B***, PPF was also examined in area CA1 (0.01 Hz stimulation with ISIs of 20, 50, 80, 100, 200, 300, 400, and 500 ms with electrodes placed in the outer or inner molecular layer of the piriform cortex). PPF ratio was calculated by dividing the amplitude of the second fEPSP by the amplitude of the first fEPSP. PPF was not affected in *CRMP-1*$^{+/-}$ or *CRMP-1*$^{-/-}$ mice. *n*, Number of slices; *N*, number of mice.

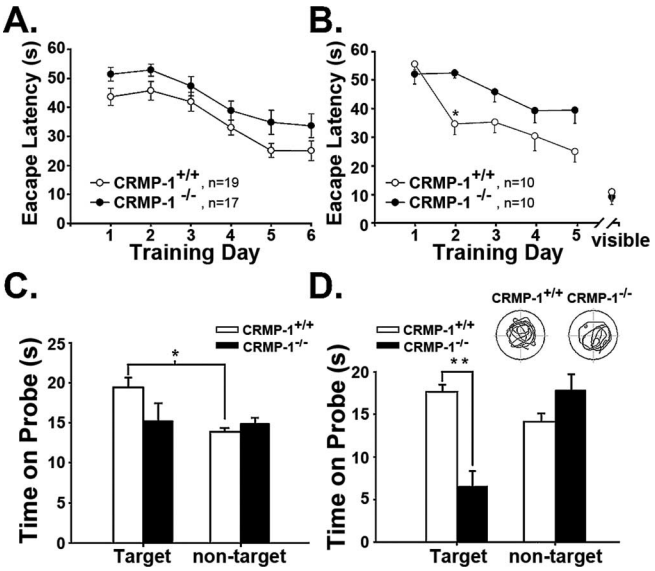

Figure 7. Impaired spatial learning and memory performance in *CRMP-1*$^{-/-}$ mice. Young adult (8–12 weeks of age) (***A***, ***C***) and aged (5–10 months) (***B***, ***D***) mice were tested in the Morris water maze. ***A***, ***B***, Latency to find the hidden platform by young adult (***A***) and aged (***B***) wild-type (*CRMP-1*$^{+/+}$) and *CRMP-1*$^{-/-}$ mice. *CRMP-1*$^{-/-}$ mice showed a delayed escape latency for the daily training trials compared with *CRMP-1*$^{+/+}$ mice (one-way ANOVA followed by *post hoc* Scheffé's test; ANOVA, $p < 0.01$ for ***A***; ANOVA, $p < 0.001$, and *post hoc*, $^{*}p < 0.05$ for ***B***). ***C***, ***D***, Probe tests for retention in adult (***C***) and aged (***D***) mice. *CRMP-1*$^{+/+}$ mice spent more time in the target than in a nontarget quadrant ($^{*}p < 0.005$), whereas *CRMP-1*$^{-/-}$ mice showed no difference in the target and nontarget quadrant. ***D***, Averaged time spent in the target quadrant was 16.65 and 6.55 s for *CRMP-1*$^{+/+}$ and *CRMP-1*$^{-/-}$ mice, respectively ($^{**}p < 0.0001$). Error bars indicate SEM.

cause CRMP-1 interacts with tubulin dimers as CRMP-2 does, CRMP-1 may also act as a cargo adapter linking the tubulin dimer or the MAPs to regulate their transport in neurites (Arimura and Kaibuchi, 2005). No overall difference between wild-type and mutant MAP2 levels in the hippocampus were detected by Western blot experiments, suggesting that MAP2 expression was not downregulated in the mutants, but rather it failed to be transported into the distal dendrites.

Unlike in CA1, MAP2 expression in the cortex and cerebellum were indistinguishable between wild-type and mutant mice (Fig. 5). This regional dissociation together with the overall higher CRMP-1 levels in the hippocampus (Fig. 2) suggests that CRMP-1 may play a more perceptible role in the hippocampus than in the cortex or cerebellum. The observations that LacZ staining was not detected in the hippocampus or cortex of P1~P21 mice with LacZ knock-in in CRMP-1 gene locus, but became clearly apparent in the hippocampus while faintly visible in the cortex of adult mice (Charrier et al., 2006), and that the LacZ knock-in had negligible effects in cerebellum (Charrier et al., 2006; Yamashita et al., 2006), are consistent with our hypothesis above.

We observed that *CRMP-1*$^{-/-}$ mice had reduced PSD95 immunolabeling (Figs. 4*d–f*, 5), indicative of fewer dendritic spines, and diffuse GAP-43 labeling, indicative of fewer growth cones (Figs. 4*g–i*, 5), as well as decreased PDS95 and GAP-43 protein levels in CA1 stratum radiatum. GAP-43 knock-out mice have severe defects and poor survival (Strittmatter et al., 1995). GAP-43 heterozygotes show abnormal pathfinding of thalamocortical afferents neonatally, but appear normal as adults, apparently rescued, at least in part, by prolonged GAP-43 expression (McIlvain and McCasland, 2006). We estimated that *CRMP-1*$^{-/-}$ mice had nearly 56% wild-type PSD95 and 50% wild-type GAP-43 levels in the hippocampus. Although we did not detect CRMP-1 in the axons by immunohistochemistry as previous work did not either (Bretin et al., 2005), our study corroborated previous work showing CRMP-1 expression in primary cultures of cortical neurons (Bretin et al., 2005), where the developmentally critical GAP-43 protein is prominent, that there may be an interaction between CRMP-1 and GAP-43 expression during axonal development.

Unlike in CA1, MAP2, PSD95, and GAP-43 immunoreactivity patterns in the *CRMP-1*$^{-/-}$ mice in CA3 and DG appeared normal (data not shown). We did not observe Tau-MAP2 or Tau-PSD95 colocalization in the CA1, CA3, or DG of wild-type or knock-out mice. Thus, the absence of dislocated or abnormally

phosphorylated Tau indicates that the CRMP$^{-/-}$ phenotype is not attributable to altered Tau-mediated microtubule activities. Double immunohistochemistry for Tau-1 (axon specific marker) and synapsin I did not reveal differences between wild-type and mutant mice in CA1, CA3, or DG (Fig. 5*A*). This is not surprising because CRMP-1 is not detected in axons by immunohistochemistry (Bretin et al., 2005; this study) and Tau-knock-out mice show normal MAP2, GAP-43, and synaptophysin immunoreactivity in hippocampus (Dawson et al., 2001).

MAP2 stabilizes microtubules (Ozer and Halpain, 2000) and its association with the cytoskeleton is important for neurite outgrowth and synaptic plasticity (Sanchez et al., 2000). Given that MAP2 is present postsynaptically and in dendritic spines (Morales and Fifkova, 1989) and that modifications in cytoskeletal dynamics are critical in the synaptic changes that occur during LTP formation, it is plausible that MAP2 may influence cytoskeletal dynamics during neuronal plasticity (Kaech et al., 2001). Indeed increased MAP2 modification has been correlated to LTP induction in the hippocampus (Roberts et al., 1998). Thus, inappropriate localization of MAP2 in *CRMP-1*$^{-/-}$ mice might alter LTP formation via effects on cytoskeletal dynamics. Meanwhile, GAP-43 is presynaptically localized and its expression is upregulated during axonal outgrowth (Benowitz and Routtenberg, 1997). Transcription and phosphorylation of GAP-43 are increased after LTP (Lovinger et al., 1985), and manipulating GAP-43 levels can alter LTP and regulate synaptic enhancement (Namgung et al., 1997). Because hippocampal dendritic spine density reflects the number of excitatory synapses per neuron associated with learning (Moser et al., 1994), we posit that reduction of hippocampal PSD95 and GAP-43 represent a reduction of dendritic spine density associated with impaired neuronal plasticity, which in turn may contribute to cognitive deficits.

Both young and old *CRMP-1*$^{-/-}$ mice exhibited impaired spatial memory performance. This impairment may be directly related to diminished hippocampal LTP. PPF is considered to be a useful test for detecting altered neurotransmitter release because the facilitation of the second response in PPF is attributed to residual presynaptic Ca^{2+} (Debanne et al., 1996). Thus, our finding that *CRMP-1*$^{-/-}$ mice exhibited normal PPF indicates that CRMP-1 deficiency does not affect transmitter release in response to twin pulses. However, GAP-43 is a PKC (protein kinase C) substrate and colocalizes with actin, which has been suggested to play an important role in facilitating the movement of reserve pools of transmitter vesicles to the readily releasable state. Therefore, an inhibitory effect on transmitter release with reduced GAP-43 cannot be excluded (Biewenga et al., 1996; Iannazzo, 2001).

Although CRMP-1 is widely expressed in the nervous system (Ricard et al., 2000; Veyrac et al., 2005), we did not observe abnormal neural marker expression in the cerebellum (data not shown), abnormal spontaneous locomotor activity, nor any evidence of general motor or sensory deficits in *CRMP-1*$^{-/-}$ mice. Thus, the *CRMP-1*$^{-/-}$ phenotype was in agreement with the finding that adult CRMP locus LacZ knock-in mice had a normal cerebellum (Charrier et al., 2006).

Summary and future directions

Herein, we present the first evidence showing that CRMP-1 is involved in spatial learning and hippocampal plasticity. We also demonstrated altered MAP2, PSD95, and GAP-43 expression patterns in *CRMP-1*$^{-/-}$ mice. Whether CRMP-1 affects other aspects of behavior or regulates neuronal structure and plasticity in other regions remains to be determined. In the future, we plan to investigate the role of CRMP-1 in areas of the nervous system where CRMP-1 is expressed constitutively with *CRMP-1*$^{fl/fl}$ mice generated in our laboratory.

References

Arimura N, Kaibuchi K (2005) Key regulators in neuronal polarity. Neuron 48:881–884.

Benowitz LI, Routtenberg A (1997) GAP-43: an intrinsic determinant of neuronal development and plasticity. Trends Neurosci 20:84–91.

Biewenga JE, Schrama LH, Gispen WH (1996) Presynaptic phosphoprotein B-50/GAP-43 in neuronal and synaptic plasticity. Acta Biochim Pol 43:327–338.

Bretin S, Reibel S, Charrier E, Maus-Moatti M, Auvergnon N, Thevenoux A, Glowinski J, Rogemond V, Premont J, Honnorat J, Gauchy C (2005) Differential expression of CRMP1, CRMP2A, CRMP2B, and CRMP5 in axons or dendrites of distinct neurons in the mouse brain. J Comp Neurol 486:1–17.

Brown M, Jacobs T, Eickholt B, Ferrari G, Teo M, Monfries C, Qi RZ, Leung T, Lim L, Hall C (2004) α2-chimaerin, cyclin-dependent kinase 5/p35, and its target collapsin response mediator protein-2 are essential components in semaphorin 3A-induced growth-cone collapse. J Neurosci 24:8994–9004.

Byk T, Dobransky T, Cifuentes-Diaz C, Sobel A (1996) Identification and molecular characterization of Unc-33-like phosphoprotein (Ulip), a putative mammalian homolog of the axonal guidance-associated unc-33 gene product. J Neurosci 16:688–701.

Byk T, Ozon S, Sobel A (1998) The Ulip family phosphoproteins—common and specific properties. Eur J Biochem 254:14–24.

Charrier E, Mosinger B, Meissirel C, Aguera M, Rogemond V, Reibel S, Salin P, Chounlamountri N, Perrot V, Belin MF, Goshima Y, Honnorat J, Thomasset N, Kolattukudy P (2006) Transient alterations in granule cell proliferation, apoptosis and migration in postnatal developing cerebellum of CRMP1(−/−) mice. Genes Cells 11:1337–1352.

Chen H, Bagri A, Zupicich JA, Zou Y, Stoeckli E, Pleasure SJ, Lowenstein DH, Skarnes WC, Chedotal A, Tessier-Lavigne M (2000) Neuropilin-2 regulates the development of selective cranial and sensory nerves and hippocampal mossy fiber projections. Neuron 25:43–56.

Cheng HJ, Bagri A, Yaron A, Stein E, Pleasure SJ, Tessier-Lavigne M (2001) Plexin-A3 mediates semaphorin signaling and regulates the development of hippocampal axonal projections. Neuron 32:249–263.

Cole AR, Causeret F, Yadirgi G, Hastie CJ, McLauchlan H, McManus EJ, Hernandez F, Eickholt BJ, Nikolic M, Sutherland C (2006) Distinct priming kinases contribute to differential regulation of collapsin response mediator proteins by glycogen synthase kinase-3 in vivo. J Biol Chem 281:16591–16598.

Dawson HN, Ferreira A, Eyster MV, Ghoshal N, Binder LI, Vitek MP (2001) Inhibition of neuronal maturation in primary hippocampal neurons from tau deficient mice. J Cell Sci 114:1179–1187.

Debanne D, Guerineau NC, Gahwiler BH, Thompson SM (1996) Paired-pulse facilitation and depression at unitary synapses in rat hippocampus: quantal fluctuation affects subsequent release. J Physiol (Lond) 491:163–176.

Deo RC, Schmidt EF, Elhabazi A, Togashi H, Burley SK, Strittmatter SM (2004) Structural bases for CRMP function in plexin-dependent semaphorin3A signaling. EMBO J 23:9–22.

D'Hooge R, De Deyn PP (2001) Applications of the Morris water maze in the study of learning and memory. Brain Res Brain Res Rev 36:60–90.

Eddy NB, Leimbach D (1953) Synthetic analgesics. II. Dithienylbutenyl- and dithienylbutylamines. J Pharmacol Exp Ther 107:385–393.

Fukada M, Watakabe I, Yuasa-Kawada J, Kawachi H, Kuroiwa A, Matsuda Y, Noda M (2000) Molecular characterization of CRMP5, a novel member of the collapsin response mediator protein family. J Biol Chem 275:37957–37965.

Fukata Y, Itoh TJ, Kimura T, Menager C, Nishimura T, Shiromizu T, Watanabe H, Inagaki N, Iwamatsu A, Hotani H, Kaibuchi K (2002) CRMP-2 binds to tubulin heterodimers to promote microtubule assembly. Nat Cell Biol 4:583–591.

Gaetano C, Matsuo T, Thiele CJ (1997) Identification and characterization of a retinoic acid-regulated human homologue of the unc-33-like phosphoprotein gene (hUlip) from neuroblastoma cells. J Biol Chem 272:12195–12201.

Good PF, Alapat D, Hsu A, Chu C, Perl D, Wen X, Burstein DE, Kohtz DS

(2004) A role for semaphorin 3A signaling in the degeneration of hippocampal neurons during Alzheimer's disease. J Neurochem 91:716–736.
Goshima Y, Nakamura F, Strittmatter P, Strittmatter SM (1995) Collapsin-induced growth cone collapse mediated by an intracellular protein related to UNC-33. Nature 376:509–514.
Gu Y, Ihara Y (2000) Evidence that collapsin response mediator protein-2 is involved in the dynamics of microtubules. J Biol Chem 275:17917–17920.
Gu Y, Hamajima N, Ihara Y (2000) Neurofibrillary tangle-associated collapsin response mediator protein-2 (CRMP-2) is highly phosphorylated on Thr-509, Ser-518, and Ser-522. Biochemistry 39:4267–4275.
Harada A, Teng J, Takei Y, Oguchi K, Hirokawa N (2002) MAP2 is required for dendrite elongation, PKA anchoring in dendrites, and proper PKA signal transduction. J Cell Biol 158:541–549.
Honnorat J, Byk T, Kusters I, Aguera M, Ricard D, Rogemond V, Quach T, Aunis D, Sobel A, Mattei MG, Kolattukudy P, Belin MF, Antoine JC (1999) Ulip/CRMP proteins are recognized by autoantibodies in paraneoplastic neurological syndromes. Eur J Neurosci 11:4226–4232.
Iannazzo L (2001) Involvement of B-50 (GAP-43) phosphorylation in the modulation of transmitter release by protein kinase C. Clin Exp Pharmacol Physiol 28:901–904.
Kaech S, Parmar H, Roelandse M, Bornmann C, Matus A (2001) Cytoskeletal microdifferentiation: a mechanism for organizing morphological plasticity in dendrites. Proc Natl Acad Sci USA 98:7086–7092.
Kondo S, Okuda A, Sato H, Tachikawa N, Terashima M, Kanegae Y, Saito I (2003) Simultaneous on/off regulation of transgenes located on a mammalian chromosome with Cre-expressing adenovirus and a mutant loxP. Nucleic Acids Res 31:e76.
Lee EC, Yu D, Martinez de Velasco J, Tessarollo L, Swing DA, Court DL, Jenkins NA, Copeland NG (2001) A highly efficient *Escherichia coli*-based chromosome engineering system adapted for recombinogenic targeting and subcloning of BAC DNA. Genomics 73:56–65.
Liu BP, Strittmatter SM (2001) Semaphorin-mediated axonal guidance via Rho-related G proteins. Curr Opin Cell Biol 13:619–626.
Lovinger DM, Akers RF, Nelson RB, Barnes CA, McNaughton BL, Routtenberg A (1985) A selective increase in phosporylation of protein F1, a protein kinase C substrate, directly related to three day growth of long term synaptic enhancement. Brain Res 343:137–143.
McIlvain V, McCasland JS (2006) GAP-43 heterozygous mice show delayed barrel patterning, differentiation of radial glia, and downregulation of GAP-43. Anat Rec A Discov Mol Cell Evol Biol 288:143–157.
Morales M, Fifkova E (1989) Distribution of MAP2 in dendritic spines and its colocalization with actin. An immunogold electron-microscope study. Cell Tissue Res 256:447–456.
Moser MB, Trommald M, Andersen P (1994) An increase in dendritic spine density on hippocampal CA1 pyramidal cells following spatial learning in adult rats suggests the formation of new synapses. Proc Natl Acad Sci USA 91:12673–12675.
Namgung U, Matsuyama S, Routtenberg A (1997) Long-term potentiation activates the GAP-43 promoter: selective participation of hippocampal mossy cells. Proc Natl Acad Sci USA 94:11675–11680.
Ozer RS, Halpain S (2000) Phosphorylation-dependent localization of microtubule-associated protein MAP2c to the actin cytoskeleton. Mol Biol Cell 11:3573–3587.
Quach TT, Duchemin AM, Rogemond V, Aguera M, Honnorat J, Belin MF, Kolattukudy PE (2004) Involvement of collapsin response mediator proteins in the neurite extension induced by neurotrophins in dorsal root ganglion neurons. Mol Cell Neurosci 25:433–443.
Quinn CC, Gray GE, Hockfield S (1999) A family of proteins implicated in axon guidance and outgrowth. J Neurobiol 41:158–164.
Ricard D, Stankoff B, Bagnard D, Aguera M, Rogemond V, Antoine JC, Spassky N, Zalc B, Lubetzki C, Belin MF, Honnorat J (2000) Differential expression of collapsin response mediator proteins (CRMP/ULIP) in subsets of oligodendrocytes in the postnatal rodent brain. Mol Cell Neurosci 16:324–337.
Roberts LA, Large CH, Higgins MJ, Stone TW, O'Shaughnessy CT, Morris BJ (1998) Increased expression of dendritic mRNA following the induction of long-term potentiation. Brain Res Mol Brain Res 56:38–44.
Sanchez C, Diaz-Nido J, Avila J (2000) Phosphorylation of microtubule-associated protein 2 (MAP2) and its relevance for the regulation of the neuronal cytoskeleton function. Prog Neurobiol 61:133–168.
Shih JY, Yang SC, Hong TM, Yuan A, Chen JJ, Yu CJ, Chang YL, Lee YC, Peck K, Wu CW, Yang PC (2001) Collapsin response mediator protein-1 and the invasion and metastasis of cancer cells. J Natl Cancer Inst 93:1392–1400.
Steeg PS (2001) Collapsin response mediator protein-1: a lung cancer invasion suppressor gene with nerve. J Natl Cancer Inst 93:1364–1365.
Strittmatter SM, Fankhauser C, Huang PL, Mashimo H, Fishman MC (1995) Neuronal pathfinding is abnormal in mice lacking the neuronal growth cone protein GAP-43. Cell 80:445–452.
Taniguchi M, Yuasa S, Fujisawa H, Naruse I, Saga S, Mishina M, Yagi T (1997) Disruption of semaphorin III/D gene causes severe abnormality in peripheral nerve projection. Neuron 19:519–530.
Uchida Y, Ohshima T, Sasaki Y, Suzuki H, Yanai S, Yamashita N, Nakamura F, Takei K, Ihara Y, Mikoshiba K, Kolattukudy P, Honnorat J, Goshima Y (2005) Semaphorin3A signalling is mediated via sequential Cdk5 and GSK3beta phosphorylation of CRMP2: implication of common phosphorylating mechanism underlying axon guidance and Alzheimer's disease. Genes Cells 10:165–179.
Veyrac A, Giannetti N, Charrier E, Reymond-Marron I, Aguera M, Rogemond V, Honnorat J, Jourdan F (2005) Expression of collapsin response mediator proteins 1, 2 and 5 is differentially regulated in newly generated and mature neurons of the adult olfactory system. Eur J Neurosci 21:2635–2648.
Vooijs M, Jonkers J, Berns A (2001) A highly efficient ligand-regulated Cre recombinase mouse line shows that LoxP recombination is position dependent. EMBO Rep 2:292–297.
Wang LH, Strittmatter SM (1996) A family of rat CRMP genes is differentially expressed in the nervous system. J Neurosci 16:6197–6207.
Wang LH, Strittmatter SM (1997) Brain CRMP forms heterotetramers similar to liver dihydropyrimidinase. J Neurochem 69:2261–2269.
Yadav N, Lee J, Kim J, Shen J, Hu MC, Aldaz CM, Bedford MT (2003) Specific protein methylation defects and gene expression perturbations in coactivator-associated arginine methyltransferase 1-deficient mice. Proc Natl Acad Sci USA 100:6464–6468.
Yamashita N, Uchida Y, Ohshima T, Hirai S, Nakamura F, Taniguchi M, Mikoshiba K, Honnorat J, Kolattukudy P, Thomasset N, Takei K, Takahashi T, Goshima Y (2006) Collapsin response mediator protein 1 mediates reelin signaling in cortical neuronal migration. J Neurosci 26:13357–13362.
Yu IS, Lin SR, Huang CC, Tseng HY, Huang PH, Shi GY, Wu HL, Tang CL, Chu PH, Wang LH, Wu KK, Lin SW (2004) TXAS-deleted mice exhibit normal thrombopoiesis, defective hemostasis, and resistance to arachidonate-induced death. Blood 104:135–142.
Yu Z, Kryzer TJ, Griesmann GE, Kim K, Benarroch EE, Lennon VA (2001) CRMP-5 neuronal autoantibody: marker of lung cancer and thymoma-related autoimmunity. Ann Neurol 49:146–154.